The response of mesophyll conductance to ozone-induced oxidative stress is genotype-dependent in poplar

Ricardo Joffe, Audrey Berthe, Yves Jolivet, Anthony Gandin

SOCIETY FOR EXPERIMENTAL BIOLOGY

Journal of Experimental Botany
https://doi.org/10.1093/jxb/erac154 Advance Access Publication 16 April, 2022
This paper is available online free of all access charges (see https://academic.oup.com/jxb/pages/openaccess for further details)

RESEARCH PAPER

The response of mesophyll conductance to ozone-induced oxidative stress is genotype-dependent in poplar

Ricardo Joffe, Audrey Berthe, Yves Jolivet and Anthony Gandin*

Université de Lorraine, AgroParisTech, INRAE, SILVA, F-54000 Nancy, France

* Correspondence: anthony.gandin@univ-lorraine.fr

Received 6 October 2021; Editorial decision 5 April 2022; Accepted 14 April 2022

Editor: Johannes Kromdijk, University of Cambridge, UK

Abstract

The CO_2 diffusion conductance within the leaf mesophyll (g_m) is considered a major limiting factor of photosynthesis. However, the effects of the major secondary air pollutant ozone (O_3) on g_m have been poorly investigated. Eight genotypes of the economically important tree species *Populus* × *canadensis* Moench were exposed to 120 ppb O_3 for 21 d. g_m showed a genotype-dependent response to O_3-induced oxidative stress and was a major limiting factor of net assimilation rate (A_{net}), ahead of stomatal conductance to CO_2 (g_{sc}) and of the maximum carboxylation capacity of the Rubisco enzyme (V_{cmax}) in half of the tested genotypes. Increased leaf dry mass per area (LMA) and decreased chlorophyll content were linked to the observed g_m decrease, but this relationship did not entirely explain the different genotypic g_m responses. Moreover, the oxidative stress defence metabolites ascorbate and glutathione were not related to O_3 tolerance of g_m. However, malondialdehyde probably mitigated the observed g_m decrease in some genotypes due to its oxidative stress signalling function. The large variation of g_m suggests different regulation mechanisms amongst poplar genotypes under oxidative stress.

Keywords: Genotypic variability, mesophyll conductance, oxidative stress, ozone, photosynthesis, *Populus*.

Introduction

The capacity of CO_2 to diffuse from the intercellular airspace within a leaf to the site of Rubisco carboxylation within chloroplasts is defined as mesophyll conductance (g_m) (Evans and Caemmerer, 1996). It can considerably limit photosynthesis under both stress and non-stress conditions (Evans *et al.*, 2009; Flexas et al., 2012, 2018). This limitation can be of similar or even greater magnitude than those caused by stomatal conductance (g_s), the maximum carboxylation capacity of Rubisco (V_{cmax}), or the maximum rate of electron transport (J_{max}) driving ribulose 1,5-bisphosphate (RuBP) regeneration within the Calvin–Benson cycle (Grassi and Magnani, 2005; Evans and Caemmerer, 2013; Gago *et al.*, 2020). However, the improvement of plant photosynthesis has so far mainly been focused on the modification of the stomatal dynamics or the enhancement of Rubisco capacity (Lawson and Vialet-Chabrand, 2019; South *et al.*, 2019; Flexas *et al.*, 2021). In addition, it is now broadly accepted that a meaningful quantification of photosynthetic limitation is only valid when including g_m and in turn V_{cmax} and J_{max} based on the CO_2 partial pressure in the chloroplast stroma (C_c) (Sun *et al.*, 2014a; Flexas *et al.*, 2018). Consequently, g_m was recently included in global carbon cycle models because its omission would lead to significant

Abbreviations: A_{net}, net assimilation rate; Asc, ascorbate; C_c, CO_2 partial pressure in the chloroplast; B_L, contribution of biochemical limitation to the A_{net} decrease; C_i, intercellular CO_2 partial pressure; C_i–C_c, CO_2 drawdown from the intercellular airspace to chloroplasts; g_s, stomatal conductance to water vapour; g_{sc}, stomatal conductance to CO_2; J_{1000}, electron transport rate at 1000 µmol m^{-2} s^{-1} PPFD; J_{max}, maximum electron transport rate; LMA, leaf dry mass per area; l_b, l_m, l_s, photosynthetic limitation by biochemistry, the mesophyll, stomatal conductance;MC_L, contribution of mesophyll limitation to the A_{net} decrease; MDA, malondialdehyde; S_L, contribution of stomatal conductance limitation to the A_{net} decrease; V_{cmax}, maximum carboxylation rate of the Rubisco enzyme.

underestimation of V_{cmax} and J_{max}, and of gross primary productivity (Sun et al., 2014a, b; Knauer et al., 2019, 2020).

Within short and long time periods, g_m is highly responsive to various abiotic stresses including the major secondary air pollutant ozone (O_3) (Flexas et al., 2008, 2018; Xu et al., 2019, 2020). An ever-increasing frequency of heatwaves and precursor emissions (e.g. nitrogen oxides, volatile organic compounds, CH_4, and CO) is fostering O_3 formation and thus causing higher background concentrations and more frequent events of temporary exposure to elevated O_3 levels on a global scale (Fowler *et al.*, 2008; Sicard *et al.*, 2017; Schaub *et al.*, 2018; Zhang *et al.*, 2019). O_3 is well known to generate reactive oxygen species (ROS) and ultimately oxidative stress (Gill and Tuteja, 2010; Noctor *et al.*, 2018), which decrease plant growth and productivity (Wittig *et al.*, 2009; Proietti *et al.*, 2016; Jolivet *et al.*, 2016; Paoletti *et al.*, 2020). To counteract increased levels of ROS, plants possess a pool of antioxidants, amongst which ascorbic acid and glutathione (GSH) play a predominant role in mitigating O_3 damage at the cellular level (Zechmann, 2011). The apoplastic antioxidant metabolism influences g_m by modifying the cell wall composition under salt and drought stresses (Clemente-Moreno *et al.*, 2019), suggesting an important role of the cell detoxification capacity within the g_m response to stress. Besides that, it was suggested that O_3 induces an increased synthesis of stress lignin in poplar mesophyll cells, thus increasing cell wall lignification (Cabané *et al.*, 2004). This might enhance ROS resistance either through antioxidant or a barrier effect (Pell *et al.*, 1997; Oksanen *et al.*, 2005), but also causing g_m to decline due to a higher cell wall resistance (Flexas *et al.*, 2021).

O_3 impairs photosynthesis in several species due to a negative impact on both stomatal and non-stomatal components (Wittig *et al.*, 2009; Paoletti *et al.*, 2020). At the stomata level, O_3 decreases CO_2 availability by impairing the opening–closing mechanism, leading to so-called stomatal sluggishness. This is mainly caused by a disturbed signal transduction as a result of a malfunctioning ion flux and inhibited expression of the key genes involved in the process (Dumont *et al.*, 2014). Consequently, the O_3 influx but also CO_2 uptake is reduced (Paoletti and Grulke, 2010). O_3 can have a significant effect on g_m, particularly due to changes in the structural characteristics of the leaf mesophyll (Günthardt-Goerg, 1996; Paoletti *et al.*, 2009). However, conflicting results have been obtained regarding a possible relationship between g_m and O_3-modified leaf traits (Xu et al., 2019, 2020). The biochemical capacity is substantially affected by O_3, as a large number of key enzymes within the Calvin–Benson cycle and notably the amount and capacity of Rubisco are down-regulated (Heath, 2008). Although the activity of phosphoenolpyruvate carboxylase, a cytosolic carboxylase, is in turn stimulated under O_3, it cannot compensate for the amount of CO_2 previously fixed by Rubisco (Dizengremel, 2001). However, inconsistent results have been obtained regarding the impact of O_3 on C_c-based V_{cmax} and its contribution to A_{net} limitation (Xu et al., 2019, 2020; Hoshika *et al.*, 2020). Nevertheless, a g_m-induced reduction in CO_2 availability might be more determinative than V_{cmax} in limiting A_{net} under O_3 and high temperature when g_m is included within the estimation of V_{cmax}, as suggested by Xu *et al.* (2020).

g_m shows a considerable intra- and interspecific variability depending on the taxonomic group, especially in its effect on leaf functional traits (Flexas *et al.*, 2018). The model tree poplar displays a large g_m variability under various conditions within the genus (Flexas *et al.*, 2008; Knauer *et al.*, 2019). Such differences could be useful to further enhance our general understanding of g_m by identifying the underlying factors that drive g_m regulation under stress (Elferjani *et al.*, 2021). Previous work has already found g_m to be the main factor limiting A_{net} under O_3-induced oxidative stress in a single poplar genotype (Xu *et al.*, 2019), yet its variability within the poplar genus still remains largely unclear.

Eight contrasting genotypes of the most frequently cultivated poplar hybrid in Europe, *Populus* × *canadensis* Moench (Monclus *et al.*, 2006), were exposed to chronically elevated O_3 in order to (i) quantify the impact of O_3-induced oxidative stress on g_m, (ii) characterize the assumed genotypic differences in sensitivity of g_m, (iii) obtain the magnitude of g_m limitation and its contribution to the O_3-induced decline of A_{net}, and (iv) investigate the potential link between the g_m response to O_3 and modifications of leaf traits and of the cell redox status.

Materials and methods

Plant material and ozone exposure

Cuttings of eight *Populus* × *canadensis* Moench (*Populus deltoides* × *nigra*) genotypes, Agathe F (AF), Dorskamp (DK), I-214, I45/51, Koster (KT), Oudenberg (OB), Robusta (RB), and Soligo (SL), were grown for 5 weeks in 10-litre pots filled with potting soil (Terreau Uni Alsa LFc, Gramoflor SPI Universel) on a 2-cm layer of clay pebbles, and fertilized with slow-release 13:13:13 N:P:K fertilizer (Nutricote T 100 Fertil, Boulogne-Billancourt, France). The temperature, relative humidity, and photoperiod of eight climate chambers were set at 23/18 °C (day/night), 65 ± 5% and 14 h (300 ± 30 μmol m^{-2} s^{-1} photosynthetic photon flux density (PPFD) at leaf height), respectively. The growth conditions were recorded individually in each chamber and verified to be similar throughout the growth period. Eight replicates of each genotype were evenly distributed in the eight climate chambers. After an acclimation period of 7 d, four chambers were treated daily with O_3 at 120 ± 5 ppb for 13 h per day for 21 d, whereas the other four were exposed to charcoal-filtered air. O_3 was produced from pure O_2 by an O_3 generator (OZ500, Fischer, Bonn, Germany; and CMG3-3, Innovatec II, Rheinbach, Germany). The O_3 concentration in the climate chambers was continuously monitored by an O_3 analyser (O341M, Environment S.A., Paris, France). The plants were watered daily with tap water and rotated regularly to avoid any positioning effect. All measurements and samplings were done on four biological replicates per treatment and per genotype.

Gas exchange and chlorophyll fluorescence

Gas exchange and chlorophyll fluorescence measurements were performed in a growth chamber with a LI-6400 infra-red gas analyser

(LI-COR Inc., Lincoln, NE, USA) with an integrated fluorescence chamber head (LI-6400-40). The cuvette temperature was set at 25 °C, the light intensity at 1000 µmol m^2 s^{-1}, the air flow at 300 µmol s^{-1}, the CO_2 level at 400 µbar, relative humidity between 65% and 85%, and the vapour pressure deficit was maintained below 1.2 kPa. Measurements were performed on the youngest fully expanded mature leaf of each plant after 30 min of acclimation to reach steady state of the photosynthetic parameters and during a time window that was at least between 2 h after or before the end of the photoperiod. Besides gas exchange, chlorophyll fluorescence parameters were recorded by a leaf fluorometer following a saturating pulse of 10 mmol m^2 s^{-1} for 1 s using a multiphase flash (Loriaux *et al.*, 2013). The quantum yield of photosystem II (Φ_{PSII}) was calculated according to Genty *et al.* (1989):

$$\Phi_{PSII} = \frac{(F'_m - F_s)}{F'_m} \quad (1)$$

where F_s is the steady state fluorescence under the prevailing light conditions and F_m' is the maximal fluorescence during a short saturating pulse of light. The actual photochemical efficiency under saturated light was calculated as follows:

$$F'_v/F'_m = \frac{F'_m - F'_o}{F'_m} \quad (2)$$

where F_v' is the variable fluorescence of a light-adapted leaf and F_o' is the minimal fluorescence from a light adapted leaf measured immediately after switching off the actinic light (Murchie and Lawson, 2013). The electron transport rate estimated from chlorophyll fluorescence (J_F) was calculated according to Genty *et al.* (1989) as follows:

$$J_F = \Phi_{PSII} \times PPFD \times \alpha \times \beta \quad (3)$$

where PPFD is the photosynthetically active photon flux density incident on the leaf, α is the leaf absorbance (0.87), and β is the fraction of photons absorbed by PSII (0.5).

Estimation of g_m, R_d, Γ*, C_i*, and* V_{cmax}

g_m was estimated by means of the variable J method, according to (Harley *et al.*, 1992):

$$g_m = \frac{A_{net}}{C_i - \frac{\Gamma^* (J + 8(A_{net} + R_d))}{J - 4(A_{net} + R_d)}} \quad (4)$$

where A_{net} is the net CO_2 assimilation rate, R_d is the day mitochondrial respiration, C_i is the CO_2 partial pressure in the intercellular air spaces, Γ* is the CO_2 compensation point in the absence of mitochondrial respiration, and J is the rate of photosynthetic electron transport derived from chlorophyll fluorescence (Eq. 3) and corrected based on the empirical relationship between J_F and the electron transport rate calculated from gas exchange (J_a) measured at low O_2. To account for alternative electron sinks and to convert chlorophyll fluorescence estimates of electron transport rates to the actual transport rate (J), CO_2 response curves were obtained at a 1.5% O_2 concentration to establish the relationship between J_F and J_a (Warren, 2006; Pons *et al.*, 2009). The relationship was then expressed as $J_a = b_F(J_F + c)$, where b_F (1.101 ± 0.02 in control and 1.047 ± 0.03 under O_3; Supplementary Fig. S1) is the slope of a linear relationship between J_a and J_F with the constant c. Band-broadening effects of oxygen in the measuring wavelength were corrected for according to the manufacturer's instructions (LI-6400, LI-COR). All g_m values were measured at 400 µbar ambient p_{CO2}.

The CO_2 response curves were obtained measuring A_{net} stepwise at 400, 300, 200, 150, 100, 50, 400, 600, 800, 1000, 1400, and 1800 µbar ambient p_{CO2} and a PAR of 1000 µmol m^{-2} s^{-1}. The Laisk method was used to estimate R_d and the intercellular CO_2 compensation point (C_i*), which serves as an estimate of Γ* (Warren and Dreyer, 2006). Briefly, quick CO_2 response curves were obtained by measuring A_{net} under three different irradiances (125, 250, and 500 µmol m^{-2} s^{-1}) and at 400, 250, 150, 120, 100, 80, and 60 µbar ambient p_{CO2} (only the linear section of the CO_2 curves were used for analysis). Then, R_d (0.4. in control, 0.8 µmol m^{-2} s^{-1} under O_3) and C_i* (35 µbar for both treatments) were obtained as the respective y- and x- axis coordinates of the common intersections of the fitted linear regressions (Laisk and Loreto, 1996) (Supplementary Fig. S2). The maximum carboxylation capacity of Rubisco (V_{cmax}) and the maximum electron transport rate (J_{1000}) were obtained using the FitAci function of the Plantecophys package in R (Duursma, 2015; R Core Team, 2018). Therein, the respective Michaelis–Menten constants K_c and K_o for CO_2 and O_2, were set at 259 µbar and 179 mbar, according to von Caemmerer *et al.*, (1994). The R_d and Γ* used were obtained by the Laisk method. Besides apparent $V_{cmax}(C_i)$ and $J_{1000}(C_i)$, which are based on A_{net}–C_i response curves, $V_{cmax}(C_c)$ and $J_{1000}(C_c)$ based on A_{net}–C_c response curves were also calculated using the estimated g_m.

Quantitative limitation analysis of photosynthesis

The relative A_{net} limitations due to mesophyll conductance (l_m), stomatal conductance to CO_2 (l_s), and biochemical capacity (l_b) were quantified according to Grassi and Magnani (2005) as follows:

$$l_m = \frac{g_{tot}/g_{gm} \times \partial A/\partial C_C}{g_{tot} + \partial A/\partial C_C} \quad (5)$$

$$l_s = \frac{g_{tot}/g_{gsc} \times \partial A/\partial C_C}{g_{tot} + \partial A/\partial C_C} \quad (6)$$

$$l_b = \frac{g_{tot} \times \partial A/\partial C_C}{g_{tot} + \partial A/\partial C_C} \quad (7)$$

where g_{tot} is total conductance to CO_2 between the leaf surface and carboxylation sites, calculated as $1/g_{tot} = 1/g_{sc} + 1/g_m$, and $\partial A/\partial C_c$ is the linear slope of the range from 60 to 150 µbar CO_2 within the measured A–C_c curves.

The corresponding contributions of limited g_m (MC_L), g_{sc} (S_L), and V_{cmax} (B_L) to the A_{net} decrease under O_3 exposure were calculated as:

$$MC_L = l_m \times \Delta g_m/g_m \quad (8)$$

$$S_L = l_s \times \Delta g_{sc}/g_{sc} \quad (9)$$

$$B_L = l_b \times \frac{\Delta \partial A/\partial C_C}{\partial A/\partial C_C} \quad (10)$$

where Δ is the difference between the control and O_3 groups.

Quantification of ascorbate, glutathione, and malondialdehyde by LC-MS

Leaves previously stored at −80 °C were ground in a mortar filled with liquid nitrogen. One hundred milligrams of plant powder was suspended in 1 ml of 0.2 M HCl and homogenized using a Vibration Mill Mixer (Qiagen, Venlo, The Netherlands) for 3 × 30 s. The samples were re-immersed in liquid nitrogen between each of the three 30-s runs to preserve them. The homogenates were centrifugated at 14 000 *g* at 4 °C for 15 min. Each supernatant was collected and filtered through a 0.22 µm polyvinylidene difluoride syringe filter. Ultra-HPLC analyses were performed on an Acquity Arc system (Waters Corp., Milford, MA, USA). Separation was carried out by injecting the samples on a Kinetex EVO C18 column (100 × 2.1 mm, 2.6 µm particle size, Phenomenex, Danaher Corp., Washington DC, USA) protected by a SecurityGuard ULTRA cartridge (Phenomenex). The mobile phase consisted of Milli-Q water with 0.01% (v/v) of formic acid (solvent A) and acetonitrile with 0.01% (v/v) of formic acid (solvent B) at a flow rate of 0.4 ml min^{-1}. The analytes were separated through a gradient of 0–50% acetonitrile, starting with 0% B for 1 min and reaching 50% B after 6 min. The column was washed with 95% B for 3 min, and re-equilibrated in the starting conditions for 5 min. Autosampler and column temperatures were maintained at 4 and 30 °C, respectively. The analytes were detected using an Acquity QDa mass spectrometer equipped with a ZSpray electrospray ionization source (Waters Corp.). Ionization was operated in the negative mode to identify and quantify the reduced and oxidized forms of ascorbate (*m/z* 176.1 and 174.1, respectively) and in the positive mode for malondialdehyde (*m/z* 72.1) and the reduced and oxidized forms of glutathione (*m/z* 308.3 and 613.6, respectively). Ascorbate, glutathione, and malondialdehyde were quantified using MassLynx Software (Waters Corp.) by measuring the area of the peak corresponding to each analyte. Standard solutions at 0.5 mM for the reduced from of ascorbate (ASA), oxidized from of ascorbate (DHA), and reduced form of glutathione (GSH), and 0.01 mM for the oxidized form of glutathione (GSSG) in 0.2 M HCl were freshly prepared and analysed in the same conditions as the samples to determine the concentrations of each component in the plant tissue extracts.

Chlorophyll and flavonol contents

Chlorophyll and flavonol contents were measured using a Dualex Scientific portable leaf-clip meter (Force-A, Orsay, France). The values were the means of four different areas across the leaf. The Dualex device measured the transmitted light in the far-red (~720 nm) and near-infrared spectra (~820 nm). Then, the chlorophyll content was calculated as the transmittance ratio of these two wavelengths. The flavonol content was assessed by sequential measurement of leaf fluorescence at 375 nm and 650 nm, in relative absorbance units.

Plant and leaf traits

Poplar shoot height and diameter, number of leaves, total leaf area, and leaf and stem fresh weight were measured before and after O_3 treatment. Leaves and shoots were dried at 65 °C for 4 d, and dry weight was measured. The total leaf area of each plant was measured using a LI-3050A planimeter (LI-COR). The leaf mass per area (LMA) was calculated as leaf dry mass (g)/total leaf area (m^2).

Statistical analyses

All statistical analyses were performed in R (R Core Team, 2018). A two-way ANOVA (*emmeans* (Lenth *et al.*, 2018) and *rstatix* (Kassambara, 2020) packages) was run with genotype and treatment as factors to test their effects on the different parameters. The ANOVA assumptions of normality and homoscedasticity were checked by performing a Shapiro test and a Levene test, respectively. When requirements were not met, the data were log-transformed. In the case of a significant effect, a *post hoc* analysis was performed using a Tukey multiple pairwise comparison test using the *glht* function (*multcomp* package; Hothorn *et al.*, 2009) to obtain the significantly different subsets. The statistical relationships between treatments and genotypes were explored by linear and non-linear regression analyses, depending on which model fitted best. For each correlation, the Pearson correlation coefficient, the coefficient of determination, and the respective *P*-values were obtained using the *ggscatter* function (*ggpubr* package; Kassambara and Kassambara, 2020) and Microsoft Office Excel, 2019.

Results

Different responses of g_m and g_{sc} to O_3

Mesophyll (g_m), stomatal (g_{sc}), and total (g_{tot}) conductance to CO_2 were estimated in eight *Populus*×*canadensis* Moench genotypes exposed to O_3 or charcoal-filtered air (Fig. 1A–C). In the control plants, g_m was on average 0.24 mol m^{-2} s^{-1} bar^{-1} (min. 0.18 ± 0.02 in I214; max. 0.29 ± 0.05 in AF) (Fig. 1A). The g_m response to O_3 was characterized by genotypic variability: AF, I214, I45/51, KT, RB, and SL displayed a significant average decrease of 61% whereas DK and OB were not significantly affected. The maximum and minimum O_3-induced g_m decreases were 72% in SL and 31% in DK. To account for potential error in the parameterization of the model and in the determination of g_m, a sensitivity analysis was performed, varying Γ* and *J* accordingly, which confirmed the large decrease in g_m under O_3 and genotypic variability when assuming a ±10% error (Supplementary Tab. S1). No major differences were observed in the Γ* value determined with the Laisk method, neither between genotypes nor between treatments. In addition, there was an overall good fit of the linear portion of the curves in all genotypes (Supplementary Fig. S2).

Stomatal conductance to CO_2 (g_{sc}) was 0.22 ± 0.01 mol m^{-2} s^{-1} on average in the control plants, and 0.15 ± 0.01 mol m^{-2} s^{-1} in the O_3-treated plants (Fig. 1B), with all genotypes significantly affected. The O_3-induced g_{sc} decrease ranged from 54% in AF to 15% in RB. The response of g_{tot} to O_3 also showed genotypic variability as all genotypes except DK were significantly affected (Fig. 1C). SL was the most affected genotype, with a 63% decrease.

O_3 affects photosynthesis in poplar genotypes

The net assimilation rate (A_{net}) was 22.3 ± 0.75 µmol m^{-2} s^{-1} on average in the control plants (min. 18.12 in AF; max. 25.02 in SL) (Fig. 2A). Under O_3 exposure, the average value decreased by 30% to 15.5 ± 0.74 µmol m^{-2} s^{-1} (min. 12.88 in AF; max. 19.8 in DK). Thus, DK showed the lowest decrease (15%) and SL the highest (47%). Stomatal conductance to water vapour (g_s) was 0.35 ± 0.02 mol m^{-2} s^{-1} in the control plants and 0.24 ± 0.02 mol m^{-2} s^{-1} under O_3 exposure, and hence a 32% decrease on average (Supplementary Fig. S3).

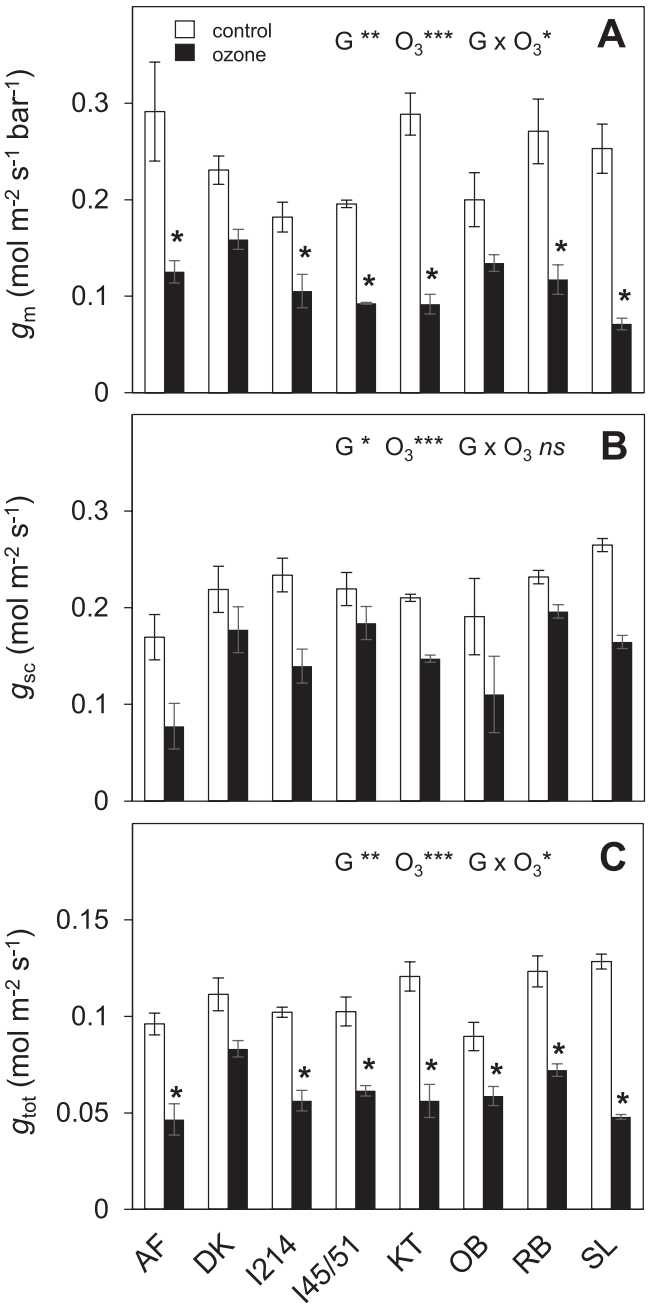

Fig 1. Mesophyll conductance (g_m, A), stomatal conductance to CO_2 (g_{sc}, B), and total conductance (g_{tot}, C) of eight *Populus* × *canadensis* Moench genotypes, Agathe F (AF), Dorskamp (DK), I-214, I45/51, Koster (KT), Oudenberg (OB), Robusta (RB), and Soligo (SL), exposed to filtered air (control) or elevated O_3 (ozone) and measured at 1000 µmol m^{-2} s^{-1} PPFD and 400 µbar CO_2 partial pressure (mean ±SE; *n*=4). Statistical results of a two-way ANOVA: G, genotype; O_3, treatment; and G×O_3, interaction between the two factors (*P≤0.05, **P≤0.01, ***P≤0.001; ns, non-significant). Significant effects of the O_3 treatment are indicated with a single asterisk when the G×O_3 interaction was significant (P<0.05).

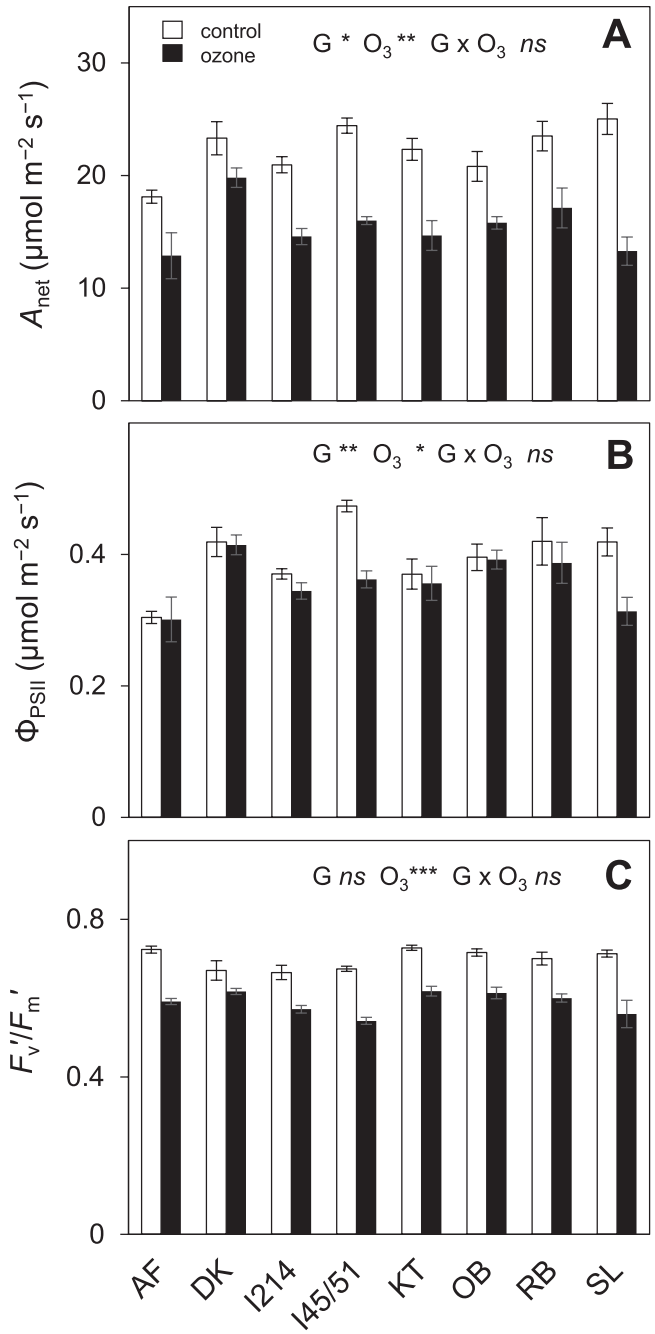

Fig 2. Net assimilation rate (A_{net}, A), quantum yield of photosystem II (Φ_{PSII}, B), and photochemical efficiency of PSII under saturated light (F_v'/F_m', C) of eight *Populus* × *canadensis* Moench genotypes exposed to filtered air (control) or elevated O_3 (ozone) measured at 1000 µmol m^{-2} s^{-1} PPFD and 400 µbar CO_2 partial pressure (mean ±SE; *n*=4). Statistical results of a two-way ANOVA. G, genotype; O_3, treatment; and G×O_3, interaction between the two factors (*P≤0.05, **P≤0.01, ***P≤0.001; ns, non-significant). Significant effects of the O_3 treatment are indicated with a single asterisk when the G×O_3 interaction was significant (P<0.05). Genotype abbreviations as in Fig. 1.

However, this decrease ranged from 15% in RB to 54% in AF. The quantum yield of photosystem II (Φ_{PSII}) was affected under O_3 exposure, with I45/51 and SL showing the greatest decreases (23% and 25%, respectively) (Fig. 2C). The efficiency of PSII under saturated light (F_m'/F_v') was 0.70 ± 0.02 on average in the control plants versus 0.59 ± 0.02 under O_3 exposure, amounting to a significant 16% decrease (Fig. 2D).

Effect on CO_2 partial pressure at the leaf intercellular airspace and at the carboxylation sites in the chloroplasts

The CO_2 partial pressures within the intercellular airspace (C_i) and the chloroplast (C_c) and their difference (C_i-C_c) were characterized by a genotype-dependent response under O_3 exposure (Fig. 3A–C). C_i was significantly affected by O_3 only in AF (−23%), while all other genotypes remained unaffected (Fig. 3A). C_c was 167.23 ± 6.74 µbar on average in the control plants, but decreased by 29% to 118.95 ± 4.73 µbar under O_3 exposure (Fig. 3B). All genotypes except I45/51 showed a significant decrease. AF showed the maximum one (45%). C_i-C_c was 100.4 ± 5.71 µbar on average in the control plants, and increased by 45% to 145.4 ± 9.51 µbar under O_3 exposure (Fig. 3C). Yet, only I45/51, RB, SL, and KT were significantly affected; KT showed the greatest increase (104%).

Different responses of C_i and C_c-based V_{cmax}

The maximum carboxylation rate of Rubisco (V_{cmax}) was estimated based on the CO_2 partial pressure within the chloroplast $V_{cmax}(C_c)$ or within the leaf intercellular airspace $V_{cmax}(C_i)$. $V_{cmax}(C_i)$ is also referred to as the apparent carboxylation rate. It was 101.2 ± 3.29 µmol m^{-2} s^{-1} on average in the control plants and decreased by 34% to 66.9 ± 4.06 µmol m^{-2} s^{-1} under O_3 exposure (Fig. 4A). Genotypic variability of $V_{cmax}(C_i)$ was high: all genotypes except AF and DK showed a significant decrease under O_3 exposure due to their lower initial slope (Supplementary Fig. S4). SL showed the highest O_3-induced decrease of $V_{cmax}(C_i)$ (53%). In contrast, $V_{cmax}(C_c)$ was not significantly impaired by O_3 exposure but the genotypes I45/51 and RB did show a decrease under O_3. Moreover, $V_{cmax}(C_c)$ was significantly higher than $V_{cmax}(C_i)$ ($P<0.001$) in both the treated and control groups (Fig. 4A, B; Supplementary Fig. S5). The C_c-based electron transport rate ($J_{1000}(C_c)$) and the $J_{1000}(C_c)/V_{cmax}(C_c)$ ratio were not significantly affected by O_3 either, but the genotypes I45/51 and RB showed a considerable decrease of ($J_{1000}(C_c)$) as well (Fig. 4C, D).

Impaired g_m was most limiting for A_{net} under O_3 exposure in most of the genotypes

The estimation of the three A_{net} limitations yielded a similar range of 34 ± 1.5% for l_m, 36 ± 1.2% for l_s and 30 ± 1.1% for l_b on average in the control (Fig. 5A–C). However, l_m increased significantly in I45/51, KT, RB, and SL under O_3 exposure (Fig. 5A), while l_s remained unchanged whatever the genotype (Fig. 5B). In contrast, l_b decreased significantly under O_3 exposure in all genotypes except I45/51 and OB (Fig 5C). The contribution of g_m (MC_L) to A_{net} was highest in I45/51, KT, and SL under O_3 exposure, while g_{sc} (S_L) was the main cause

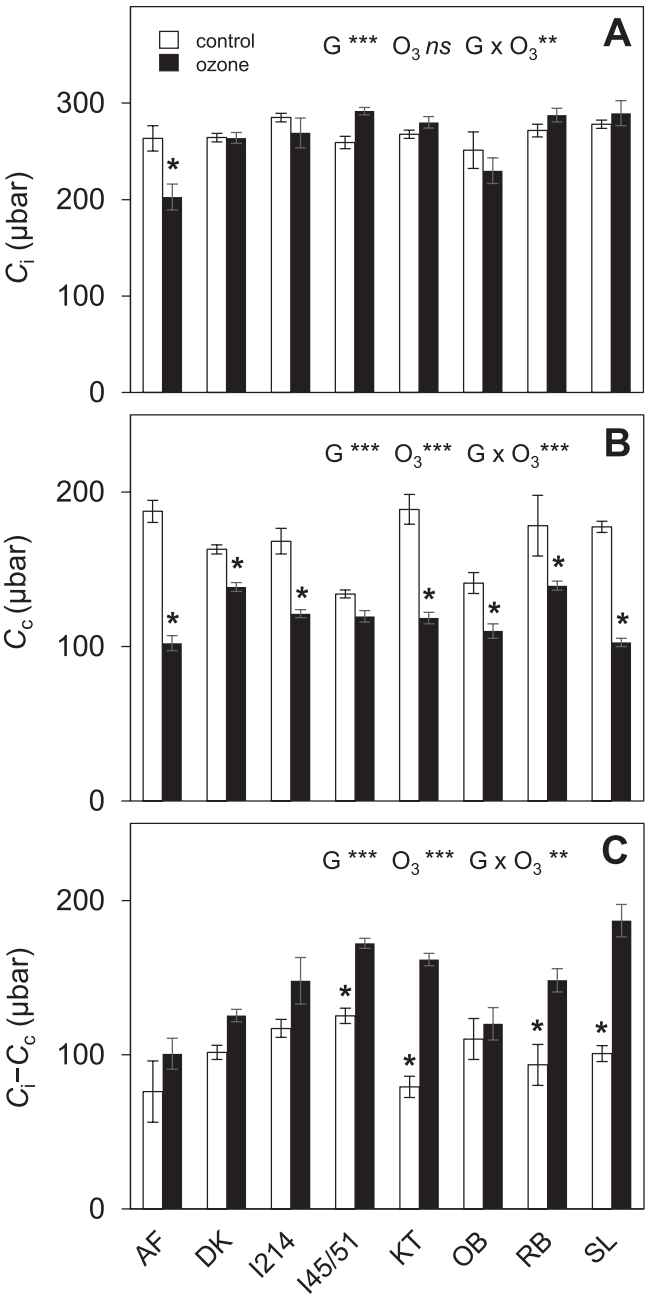

Fig 3. CO_2 partial pressure in the leaf intercellular airspace (C_i, A), at the chloroplast sites (C_c, B), and gradient between the two sites (C_i–C_c, C) of eight *Populus* × *canadensis* Moench genotypes exposed to filtered air (control) or elevated O_3 (ozone) (mean ±SE; n=4). Statistical results of a two-way ANOVA. G, genotype; O_3, treatment; and G×O_3, interaction between the two factors (*P≤0.05, **P≤0.01, ***P≤0.001; ns, non-significant). Significant effects of the O_3 treatment are indicated with a single asterisk when the G×O_3 interaction was significant (P<0.05). Genotype abbreviations as in Fig. 1.

of the A_{net} decrease in the sole AF (Fig. 5D). In comparison, the biochemical capacity (B_L) contributed only marginally to the A_{net} decrease in DK and I214, while RB showed a rather evenly distributed share of contributions. In OB, MC_L, and S_L

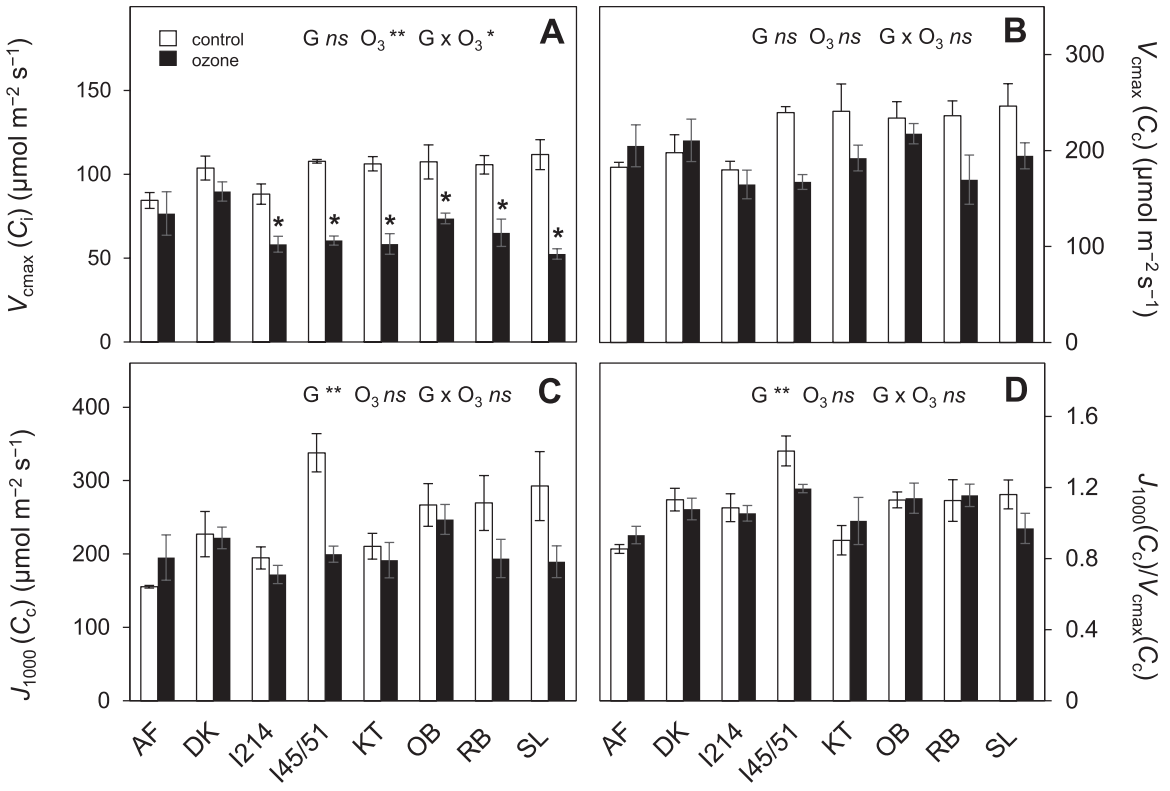

Fig 4. C_i-based ($V_{cmax}(C_i)$, A) and C_c-based ($V_{cmax}(C_c)$, B) maximum carboxylation velocity of Rubisco, C_c-based electron transport rate at 1000 µmol m^{-2} s^{-1} PPFD ($J_{1000}(C_c)$, C), and $J_{1000}(C_c)/V_{cmax}(C_c)$ ratio (D) of eight *Populus* × *canadensis* Moench genotypes exposed to filtered air (control) or elevated O_3 (ozone) (mean ±SE; n=4). Statistical results of a two-way ANOVA. G, genotype; O_3, treatment; and G×O_3, interaction between the two factors (*P≤0.05, **P≤0.01, ***P≤0.001; ns, non-significant). Significant effects of the O_3 treatment are indicated with a single asterisk when the G×O_3 interaction was significant (P<0.05). Genotype abbreviations as in Fig. 1.

equally contributed to the A_{net} decrease under O_3 exposure, but to a greater extent than B_L did.

Changes in antioxidant capacity under O_3 exposure

The content of the oxidative stress marker malondialdehyde (MDA) increased by 77 ± 9% on average under O_3 exposure (Fig. 6A). The highest MDA levels were found in DK, I214, RB, and OB, and the lowest ones in AF and SL. The flavonol content also increased by 26 ± 6% on average under O_3 exposure, ranging from 7% in RB to 58% in KT (Fig. 6B). The total contents of ascorbate and its reduced (AsA) and oxidized (DHA) forms were not significantly affected by O_3 exposure (Fig. 6C). However, the DHA contents differed considerably amongst genotypes: KT had a 2- to 3-fold higher concentration compared with DK, AF, or SL. The percentage of ASA was not affected, but also showed genotypic differences: RB displayed the lowest value and DK the highest one (Fig. 6E). In contrast, the total glutathione pool increased significantly by 13 ± 4% on average (Fig. 6D). The reduced form (GSH) showed a 15 ± 4% increase ranging from 5% in RB to 35% in SL, while an average 28 ± 7% decrease was found for the oxidized form (GSSG), ranging from 17% in DK to 46% in RB. The percentage of GSH increased significantly by 3 ± 0.5%, yet without any significant difference among genotypes (Fig. 6F).

Leaf traits affected, height growth unaffected

Leaf mass per area (LMA) increased by 18 ± 2% on average under O_3 exposure, ranging from 10% in RB to 27% in I214 (Table 1). The chlorophyll content decreased significantly by 21 ± 2% on average, from 10% in OB to 29% in KT (Table 1). The C-to-N ratio decreased by 39 ± 3% on average, from 27% in RB to 56% in KT (Table 1). The number of leaves was on average 41 ± 3% lower compared with the control plants, except in AF and I45/51, which were not significantly affected. A decrease of the mean individual leaf area (MILA) of 16 ± 4% was observed in DK and KT (4% in DK and 38% in KT) (Table 1). Stem height and diameter as well as the daily growth rate remained unaffected but showed genotypic differences. However, total biomass decreased by 34 ± 3% on average, with minimum and maximum decreases of 22% and 49% for I45/51 and KT, respectively. The highest absolute biomass was measured in DK, and the lowest one in KT (Table 1).

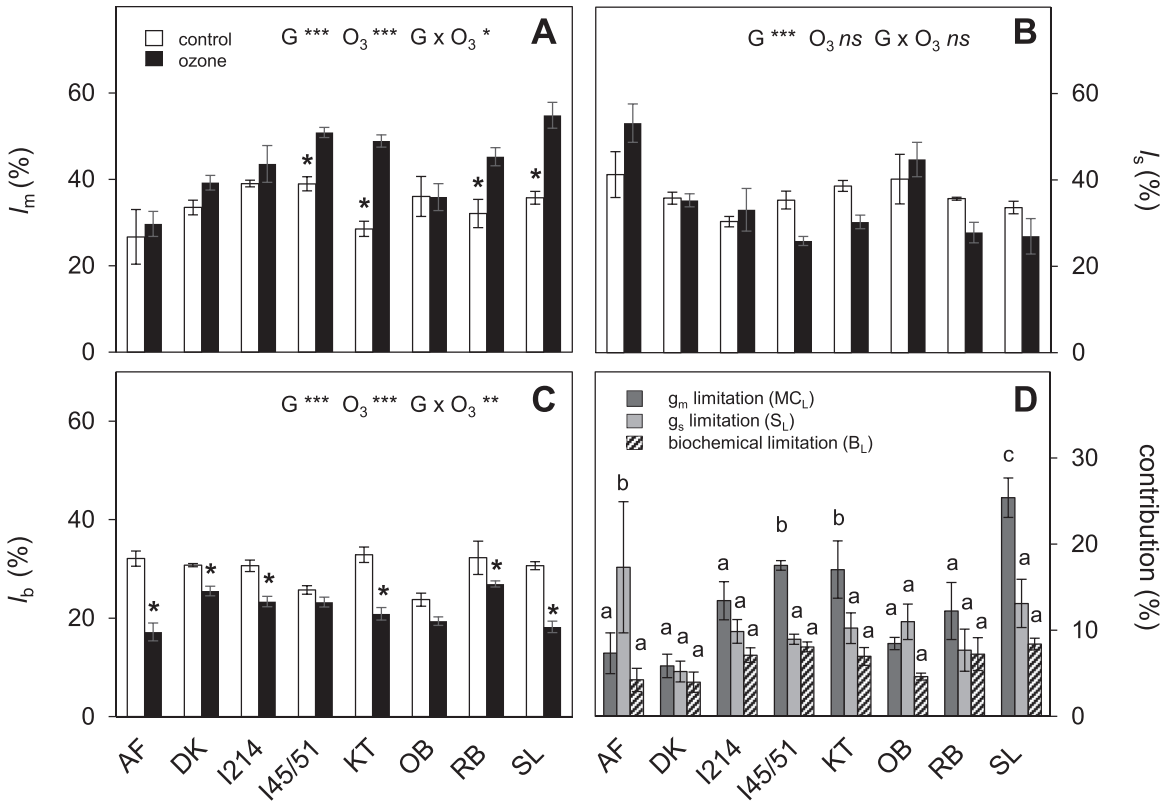

Fig 5. Relative limitations of the net assimilation rate (A_{net}) by mesophyll conductance (l_m, A), stomatal conductance to CO_2 (l_s, B) and biochemistry (l_b, C), and their respective percentage contributions M_{CL}, S_L, and B_L to the A_{net} decrease (D) of eight *Populus*×*canadensis* Moench genotypes exposed to filtered air (control) or elevated O_3 (ozone) (mean ±SE; n=4). In (A–C) statistical results of a two-way ANOVA. G, genotype; O_3, treatment; and G×O_3, interaction between the two factors (*P≤0.05, **P≤0.01, ***P≤0.001; ns, non-significant). Significant effects of the O_3 treatment are indicated with a single asterisk when the G×O_3 interaction was significant (P<0.05). In (D) different letters denote significant differences between the limitations within each genotype according to Tukey's *post hoc* test. Genotype abbreviations as in Fig. 1.

Relationship between photosynthetic capacity and leaf CO_2 conductance

At g_m values below 0.26 mol m^{-2} s^{-1} bar^{-1}, A_{net} was linearly positively related to g_m across genotypes and treatments (Fig. 7A). At higher g_m, A_{net} reached a plateau while g_m was still increasing (Fig. 7A). A_{net} and g_{sc} showed a linear relationship across all genotypes as well as within each of the two treated and control groups (Fig. 7B). Total conductance, g_{tot}, comprising both g_m and g_{sc}, also showed a very strong linear relationship with A_{net} (R^2=0.83) within each group and across all genotypes (Fig. 7C).

g_m is related to LMA and chlorophyll content

g_m was negatively related to LMA changes across genotypes and the treated versus control groups (Fig. 8A). Therefore, an increased LMA was correlated to a g_m decrease. However, the decrease lessened as LMA increased. Another yet contrasting relationship was observed between the chlorophyll content and g_m, as the two parameters were positively related (Fig. 8B). As both relationships were driven by the O_3 treatment effect rather than by a genotype-dependent response, the total population trend is shown.

A genotype-dependent relationship between g_m and the MDA content

A lower g_m was to some extent related to a higher content in oxidative stress marker, i.e. MDA, when considering the entire population trend (Fig. 9). However, this relationship differed depending on the genotype, so that separate linear regressions were fitted. A first group of genotypes including SL, KT, and AF showed a severe drop of g_m as MDA increased. This group had the sharpest slopes while the increase in the MDA concentration was rather small, and was referred to as the most MDA-responsive group. A second group including DK, I214, I45/51, and OB was characterized by a moderate g_m drop despite a much higher MDA content after O_3 exposure. This group had lower slopes and is the least MDA-responsive group. RB showed an intermediate behaviour, with a significant decrease of g_m but a higher MDA content.

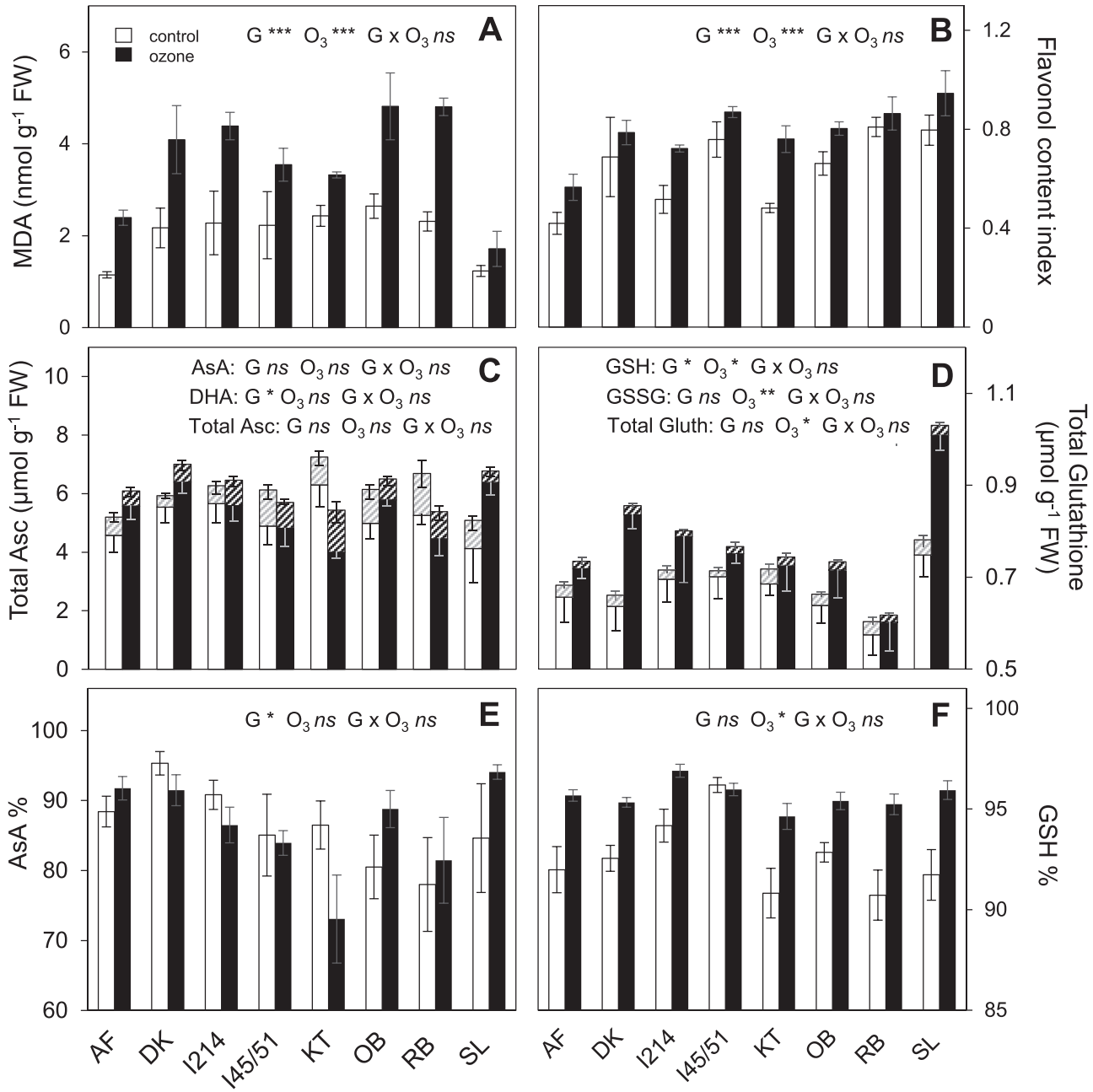

Fig 6. Contents of malondialdehyde (MDA, A), flavonol (B), ascorbate (Asc, C), and glutathione (D) and the percentages of the reduced forms of ascorbate (E) and glutathione (F) of eight *Populus* × *canadensis* Moench exposed to filtered air (control) or elevated O_3 (ozone) (mean ±SE; n=4). Ascorbate and glutathione are shown in their two forms: the upper part of the bar (diagonal stripes) represents the oxidized forms of the metabolites (DHA and GSSG, respectively), and the lower part (filled) their reduced forms. Statistical results of a two-way ANOVA. G, genotype; O_3, treatment; and G×O_3, interaction between the two factors (*P≤0.05, **P≤0.01, ***P≤0.001; ns, non-significant). Significant effects of the O_3 treatment are indicated with a single asterisk when the G×O_3 interaction was significant (P<0.05). Genotype abbreviations as in Fig. 1.

Discussion

O_3 affects g_m intra-specifically

This study is the first screening of the g_m capacity of poplar under chronically elevated O_3 and reveals a strong and genotype-dependent response of g_m to O_3-induced oxidative stress (Fig. 1A). Within the control group, a wide range of g_m values was observed amongst the *Populus* × *canadensis* Moench genotypes (0.18–0.29 µmol m^{-2} s^{-1} bar^{-1}), confirming values previously found for the *Poplar* genus (Flexas *et al.*, 2008; Soolanayakanahally *et al.*, 2009; Théroux Rancourt *et al.*, 2015).

Under O_3 exposure, g_m decreased sharply, resulting in a relative A_{net} limitation of 44% across all genotypes. Since

Table 1. Leaf traits and growth biometrics of the eight *Populus* × *canadensis* Moench genotypes exposed to filtered air (control) or elevated O_3 (O_3)

Genotype	Treatment	LMA (g m^{-2})	Chlorophyll content (μg cm^{-2})	C:N	Number of leaves	MILA (mm^2)	Final stem height (cm)	Daily growth rate (cm per day)	stem diameter (mm)	Biomass (g)
AF	Control	41.9 ± 2.1	35.4 ± 1.8	88.3 ± 7.5	32.5 ± 2.0 cd	112.1 ± 5.0	88.8 ± 5.8	2.1 ± 0.1	9.8 ± 0.3	24.3 ± 3.7
	O_3	48.3 ± 1.3	29.2 ± 0.9	53.7 ± 4.9	25.3 ± 1.1 d	91.0 ± 5.2	85.4 ± 4.2	2.1 ± 0.1	9.0 ± 0.4	18.1 ± 1.2
DK	Control	48.7 ± 2.0	40.8 ± 4.1	70.8 ± 13.3	33.8 ± 1.2 cd	194.1 ± 5.8	117.6 ± 5.1	2.7 ± 0.1	13.0 ± 0.5	52.8 ± 5.6
	O_3	57.3 ± 1.0	30.3 ± 2.1	39.0 ± 2.2	16.8 ± 1.6 ab	185.8 ± 9.9	118.8 ± 5.0	2.8 ± 0.1	15.0 ± 3.1	35.0 ± 4.3
I214	Control	44.5 ± 1.0	31.8 ± 2.4	65.0 ± 9.2	35.3 ± 2.0 d	162.5 ± 6.6	124.4 ± 6.4	2.9 ± 0.1	13.7 ± 0.6	45.2 ± 5.5
	O_3	56.5 ± 0.9	23.8 ± 1.6	33.1 ± 1.9	17.5 ± 0.8 ab	127.8 ± 10.6	128.7 ± 2.6	2.9 ± 0.0	14.1 ± 2.2	26.3 ± 3.0
I45/51	Control	50.8 ± 0.3	33.7 ± 2.9	47.0 ± 6.6	27.3 ± 0.9 b	191.2 ± 2.3	72.6 ± 1.5	2.0 ± 0.1	13.0 ± 0.2	37.0 ± 1.8
	O_3	58.0 ± 1.1	25.8 ± 1.0	29.9 ± 1.3	17.0 ± 0.7 ab	180.3 ± 9.4	74.7 ± 4.0	2.1 ± 0.1	15.2 ± 3.1	28.8 ± 2.6
KT	Control	47.1 ± 1.2	34.2 ± 2.2	72.0 ± 5.4	31.0 ± 1.2 d	107.7 ± 3.6	88.0 ± 5.1	2.6 ± 0.0	10.6 ± 0.3	23.9 ± 2.3
	O_3	54.8 ± 0.8	24.3 ± 1.6	32.7 ± 3.2	19.8 ± 1.0 ab	66.5 ± 3.5	75.9 ± 3.7	2.2 ± 0.1	10.4 ± 1.6	12.2 ± 0.8
OB	Control	48.3 ± 2.6	35.8 ± 2.5	55.2 ± 4.8	33.8 ± 1.1 d	144.5 ± 6.2	108.8 ± 2.7	2.7 ± 0.1	12.2 ± 0.5	37.5 ± 4.0
	O_3	58.0 ± 2.0	32.4 ± 2.2	40.3 ± 1.4	21.0 ± 0.4 ab	127.2 ± 5.3	109.4 ± 4.8	2.5 ± 0.1	14.0 ± 2.9	28.0 ± 2.4
RB	Control	55.2 ± 1.8	43.4 ± 2.2	55.3 ± 3.4	38.3 ± 1.8 d	146.0 ± 3.5	79.8 ± 4.0	1.7 ± 0.2	10.4 ± 1.4	44.1 ± 3.4
	O_3	60.6±.02	34.5 ± 1.6	40.5 ± 2.5	20.8 ± 0.7 b	139.0 ± 6.9	85.0 ± 3.1	1.8 ± 0.1	9.6 ± 1.1	30.4 ± 2.8
SL	Control	48.6 ± 0.6	28.9 ± 2.4	38.2 ± 4.7	25.8 ± 0.9 b	158.7 ± 10.2	69.0 ± 3.5	1.9 ± 0.1	12.0 ± 0.3	29.7 ± 3.0
	O_3	59.5 ± 2.4	22.9 ± 1.9	25.5 ± 3.5	13.3 ± 1.1 a	126.8 ± 8.1	62.2 ± 3.7	1.6 ± 0.1	9.2 ± 0.5	15.8 ± 1.8
G		***	***	***	***	***	***	***	*	***
O_3		***	***	***	***	***	ns	ns	ns	***
G×O_3		ns	ns	ns	**	ns	ns	ns	ns	ns

Values are means ±SE; n=4. Growth is shown as the daily growth rate calculated as total growth divided by the duration of the treatment. Mean individual leaf area (MILA) was calculated as the ratio of total leaf area over the number of leaves after 21 d of treatment. Asterisks show the significance of the factors/interactions: *P≤0.05, **P≤0.01, ***P≤0.001; ns, non-significant. Different letters denote significant differences between groups according to Tukey's *post hoc* test.

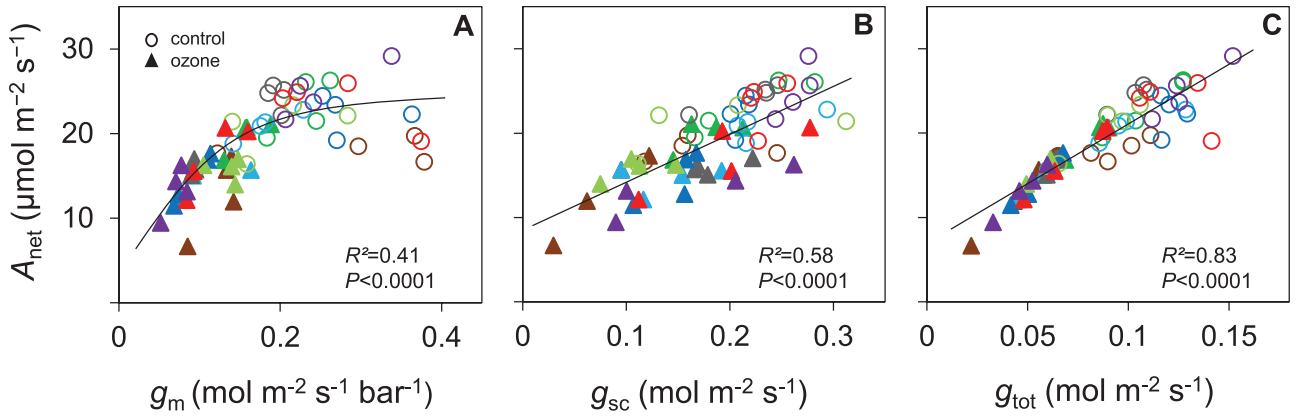

Fig 7. Relationship between the net assimilation rate (A_{net}) and mesophyll conductance (g_m, A), stomatal conductance to CO_2 (g_{sc}, B), and total conductance (g_{tot}, C) of *Populus* × *canadensis* Moench genotypes exposed to filtered air (control, circles) or elevated O_3 (ozone, triangles) (n=4). R^2 as a result of linear and non-linear regression analysis is indicated for the whole sample with the respective P-values. Colour code: AF, brown; DK, dark green; I214, bright blue; I45/51, dark grey; KT, dark blue; OB, bright green; RB, red; SL, purple.

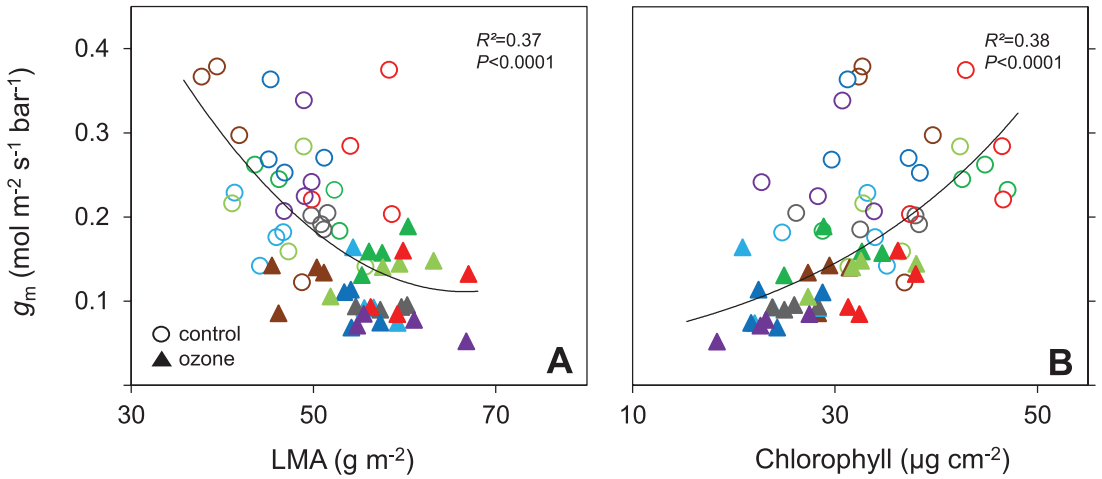

Fig 8. Relationship between mesophyll conductance (g_m) and leaf mass per area (LMA, A) and the chlorophyll content (B) of eight *Populus* × *canadensis* Moench exposed to filtered air (control, circles) or elevated O_3 (ozone, triangles) (n=4). R^2 as a result of linear and non-linear regression analysis is indicated for the whole sample with the respective P-values. Colour code: AF, brown; DK, dark green; I214, bright blue; I45/51, dark grey; KT, dark blue; OB, bright green; RB, red; SL, purple.

chlorophyll fluorescence-based g_m estimation can be subject to a significant level of uncertainty due to incorrect parameterization, particularly of Γ* and electron transport rate (J) (Walker *et al.*, 2013; Gu and Sun, 2014), a sensitivity analysis was performed that confirmed the observed g_m response in both treatments and all genotypes (Supplementary Table S1). g_m has been widely reported to respond to environmental constraints, several of which are known to induce oxidative stress (Elferjani *et al.*, 2021). A g_m decrease of a similar magnitude was recently observed in a single *Populus deltoides* hybrid grown in an open-top chamber in the long term (Xu *et al.*, 2019). However, our results also showed large genotypic variability of the g_m response to O_3, suggesting that this response was genotype-dependent amongst the cultivars. The contribution of g_m to the observed A_{net} decrease was mainly driven by genotypes I214, KT, I45/51, and notably SL, while g_{sc} and the biochemical capacity contributed in a similar proportion in DK, OB, and RB (Fig. 5D). Therefore, the contribution of g_m should be considered on a species- or genotype-dependent basis when A_{net} is limited under O_3-induced oxidative stress. In addition, as the highly g_m-limited genotypes are more susceptible to a lower A_{net} under stress conditions, they may be less suitable for cultivation in a constrained environment.

In contrast to previous studies (Harmens *et al.*, 2017; Xu et al., 2019, 2020), all poplar genotypes showed a significant g_{sc} decrease under chronic O_3 exposure (Fig. 1B). O_3-triggered stomatal closing (Dumont *et al.*, 2014) has been widely reported and suggested to be a major determinant of the photosynthetic capacity under elevated O_3. However, our study showed that l_s did not increase or only slightly increased under O_3 exposure in all genotypes but AF (Fig. 5B), suggesting

that non-stomatal A_{net} limitation can be more critical than g_{sc} (Noormets *et al.*, 2001). Consequently, as g_m was more affected than g_{sc}, O_3-induced damage of g_m-related components might have been more determinative than a reduced CO_2 uptake as a result of stomatal closure for at least half of the genotypes. Therefore, g_m should be further considered in studies assessing the photosynthetic capacity in response to O_3. Yet, the significant A_{net}–g_{tot} relationship showed a strong complementary regulation of A_{net} by both g_m and g_{sc} across genotypes and in both the treated and control plants (Fig. 7A–C). Therefore, the CO_2 pathway, consisting of g_{sc} and g_m, cannot be considered as an interdependent system affecting A_{net} to the same extent. g_m and g_{sc} each had a considerable impact on A_{net} in our study, but hardly interfered with each other.

O_3 affects the CO_2 supply to Rubisco rather than its catalytic capacity

As neither the C_c-based V_{cmax} nor J_{1000} was affected by O_3 (Fig. 4B, D), the sole biochemical limitation (B_L) contributed only marginally to the A_{net} decrease, suggesting that O_3 affected the CO_2 supply to Rubisco rather than its actual catalytic capacity. Therefore, it seems likely that C_i-based estimations of V_{cmax} presuming an undefined g_m led to an overestimation of the O_3 impact on Rubisco activity (Sun *et al.*, 2014b; Xu et al., 2019, 2020). Extensive evidence has showed that under chronic elevated O_3, the Rubisco content decreased due to a decreased expression level or a decreased protein amount (Bagard *et al.*, 2008; Dizengremel *et al.*, 2013). Nevertheless, this was highly dependent on the duration and intensity of the O_3 treatment, and Rubisco quantity and activity were not always coupled during chronic O_3 exposure (Pell *et al.*, 1992). An unaffected C_c-based V_{cmax} suggests that Rubisco or the actual number of its active sites was not limiting under our conditions compared with the low CO_2 availability caused by the observed g_m decrease. The literature is inconsistent as to the extent to which a V_{cmax} decrease is associated to a lower Rubisco content (Reid *et al.*, 1998). These discrepancies may be due to a g_m-induced limitation of CO_2 availability that is still rarely considered.

The g_m decrease under O_3 exposure is related to leaf traits

Elevated O_3 significantly decreased the chlorophyll content, and this decrease was concomitant with the observed lower g_m across all genotypes (Fig. 8B). A decreased chlorophyll content under O_3 exposure has been observed in many species including poplar (Bortier *et al.*, 2000; Ranieri *et al.*, 2001; Saitanis *et al.*, 2001; Bagard *et al.*, 2008; Xu *et al.*, 2019). This might be due to impaired CO_2 fixation and subsequent down-regulation of the electron transport chain of PSII, hence altered light-harvesting complexes, as suggested by the observed decrease of the chlorophyll fluorescence-based parameters quantum yield (Φ_{PSII}) and photochemical efficiency of PSII (F_v'/F_m') (Fig. 2B, C) (Hörtensteiner, 1999; Ranieri *et al.*, 2001; Bagard *et al.*, 2008). The latter, which describes the efficiency of the PSII reaction centre (Force *et al.*, 2003), serves also as an indicator of stress-induced changes in photosynthesis and especially in PSII (Gerosa *et al.*, 2003; Herschbach *et al.*, 2010). In this context, a decrease of the chlorophyll content under O_3 exposure can also go along with a change in the size and integrity of chloroplasts (Oksanen *et al.*, 2001; Bohler *et al.*, 2011). Furthermore, chloroplasts move within the cell under O_3 exposure (Günthardt-Goerg, 1996; Paoletti *et al.*, 2009), and this can imped the CO_2 pathway (Tholen *et al.*, 2008). Considering the widely admitted relationship between g_m and the integrity, position, and number of chloroplasts (Loreto *et al.*, 2001; Wittig *et al.*, 2007; Tosens *et al.*, 2012; Flexas et al., 2012, 2018), O_3-induced alteration of chloroplasts through degradation or altered positioning along with chlorophyll degradation may have contributed to the observed g_m decrease under our conditions.

An average LMA increase of 18% across all genotypes under O_3 exposure was linked to the observed g_m decrease (Fig. 8A). LMA is an easy-to-measure leaf structural trait that can reflect stress-induced changes in leaf anatomy (Wright *et al.*, 2005; Flexas *et al.*, 2008; Milla-Moreno *et al.*, 2016). Under O_3 exposure, a denser leaf structure can contribute to mitigating ROS damage by limiting O_3 diffusion (Emberson *et al.*, 2018) but also CO_2 diffusion. This is expected to decrease g_m. This trade-off is also observed between deciduous and evergreen species: evergreen species are generally less sensitive to O_3 (Calatayud *et al.*, 2010; Li *et al.*, 2016) and have a lower g_m (Veromann-Jürgenson *et al.*, 2017). Another anatomical change aimed at protecting cells from ROS is cell wall modification through thickening (Bussotti *et al.*, 2005) or changes in its composition, e.g. an increased lignification (Cabané *et al.*, 2004). Cell walls are therefore considered to play a central role in ROS quenching (Moldau, 1998; Oksanen *et al.*, 2001). Cell wall resistance can account for mesophyll diffusion resistance by up to 50% (Terashima *et al.*, 2011). Furthermore, up to 72% of the leaf dry mass consists of cell wall tissue, which considerably contributes to LMA (Onoda *et al.*, 2017; Ye *et al.*, 2020). Also, Sugiura *et al.* (2020) suggested a link between an increased LMA and higher cell wall mass per area and thickness which in turn cause a decrease of the chloroplastic CO_2 partial pressure. Thus, modified anatomical arrangement and/or cell wall properties aimed at protecting the plant against O_3 could increase CO_2 diffusion resistance and explain the g_m decrease observed under O_3 exposure.

The antioxidant capacity is not related to the g_m response

O_3-induced chlorophyll loss (degradation) is accompanied by an increased content in secondary metabolites such as flavonol (Bagard *et al.*, 2008; Mattila *et al.*, 2018). Flavonol substantially contributes to ROS scavenging (Dizengremel *et al.*, 2012; Zhu *et al.*, 2019), and was significantly higher under

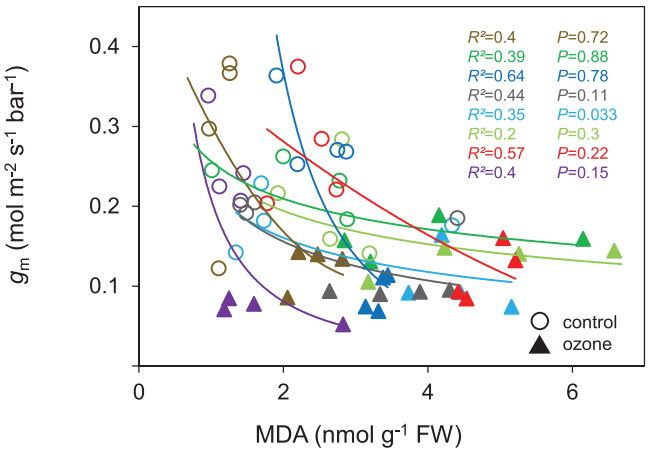

Fig 9. Relationship between mesophyll conductance (g_m) and the malondialdehyde (MDA) content of eight *Populus* × *canadensis* Moench genotypes exposed to filtered air (control, circles) or elevated O_3 (ozone, triangles) (n=4). R^2 as a result of non-linear regression analysis is indicated for each genotype with its respective P-value. Colour code: AF, brown; DK, dark green; I214, bright blue; I45/51, dark grey; KT, dark blue; OB, bright green; RB, red; SL, purple.

O_3 exposure. A large genotype-dependent difference in initial versus post-treatment flavonol contents was also observed (Fig. 6B). All genotypes also showed an increased total glutathione content, but the GSH content increased while the GSSG content decreased, suggesting *de novo* glutathione synthesis and a higher activity of glutathione reductase to sustain GSH regeneration (Fig. 6D). In contrast, the ascorbate metabolism was not affected (Fig. 6C). This is consistent with Dusart *et al.* (2019b) who found that the glutathione metabolism was responsive to O_3-induced oxidative stress in poplar. However, Clemente-Moreno *et al.* (2019) observed that apoplastic ascorbate, which travels along the CO_2 pathway, was related to the g_m response under salt and drought stress in tobacco. This was suggested to be due to a modified composition of the cell walls caused by altered apoplastic antioxidant enzyme activity, including the ascorbate redox state. A thorough analysis of apoplastic and cell compartment antioxidant levels might reveal different strategies of ROS defence and a variable impact on g_m (Kronfuß *et al.*, 1998; Haberer *et al.*, 2007; Di Baccio *et al.*, 2008; Dusart *et al.*, 2019a). In future works, an assessment of chloroplastic antioxidant pools might be of great interest to better understand the photosynthesis response to environmental constraints.

The oxidative stress marker malondialdehyde is intraspecifically linked to the g_m capacity

MDA is a lipid peroxidation marker related to redox signalling and the oxidative stress level (Farmer and Mueller, 2013). A significant MDA increase is a strong indicator of O_3-induced damage of lipid membranes. Increased MDA under chronic O_3 exposure was previously observed in poplar and other crop species (Shang *et al.*, 2020; Dai *et al.*, 2019). Amongst the eight genotypes, the MDA content was partly linked to g_m sensitivity to O_3 (Fig. 9). Accordingly, two different groups emerged. A highly MDA-responsive group showed the most severe g_m decrease along with a slight MDA increase. In contrast, a less MDA-responsive group was characterized by a moderate g_m decrease but a rather sharp MDA increase after O_3 treatment. This supports the idea that an increased amount of aldehyde compounds such as MDA is not only a sign of damage but also a key element of oxidative stress signalling allowing for the activation of ROS scavenging mechanisms, amongst others (Tagnon and Simeon, 2017; Morales and Munné-Bosch, 2019). As the MDA levels obtained in the present study were rather low in comparison with Shang *et al.*, (2020) (Fig. 6A), MDA might have acted more as a gene activator than as a damage indicator. This might explain the observed relationship between a higher MDA content and a smaller decrease of g_m under O_3 exposure in some genotypes. However, under other conditions inducing much higher MDA contents, MDA could be related to the degree of damage and thus possibly to the decreased g_m. These results provide evidence that the signalling role of MDA may be involved to some extent in the machinery regulating g_m, and impact one of its anatomical or biochemical determinants.

Conclusion

We demonstrated that the g_m response to chronic O_3-induced oxidative stress is genotype-dependent in *Populus* × *canadensis* Moench: g_m substantially contributed to the O_3-induced A_{net} decrease in half of the tested genotypes, showing that O_3 can have a greater impact on the CO_2 pathway than on the capacity of Rubisco or stomatal conductance. A relationship between the leaf traits LMA and chlorophyll content on the one hand and the g_m response on the other hand suggested a strong influence of leaf structural changes under O_3 that may in turn impair g_m. However, this relationship did not fully explain the observed intraspecific g_m response, as these traits themselves did not show a genotype-dependent response. Finally, the relationship found between the g_m capacity and the MDA content seems to support that MDA is not only a marker of the oxidative stress level but may also act as a signalling component mitigating the g_m decrease under oxidative stress. Future work could focus on multi-genotype and multi-species experiments to further decipher the determinants of the g_m response to stress, the stress-induced modification of leaf anatomical determinants of g_m, and a cell compartment-targeted analysis of antioxidants.

Supplementary data

The following supplementary data are available at *JXB* online.

Fig. S1. The relationship between rates of electron transport estimated from chlorophyll fluorescence (J_F) and calculated from gas exchange (J_a) of eight *Populus*×*canadensis* Moench genotypes exposed to filtered air or elevated O_3.

Fig. S2. Net assimilation rate (A_{net}) response to leaf internal CO_2 (C_i) under three different light conditions (Laisk method) of eight *Populus* × *canadensis* Moench genotypes exposed to filtered air or elevated O_3.

Fig. S3. Stomatal conductance to water vapour (g_s) of eight *Populus* × *canadensis* Moench genotypes exposed to filtered air or elevated O_3.

Fig. S4. A_{net}–C_i curves of eight *Populus* × *canadensis* Moench genotypes exposed to filtered air or elevated O_3.

Fig. S5. A_{net}–C_c curves of eight *Populus* × *canadensis* Moench genotypes exposed to filtered air or elevated O_3.

Table S1. Sensitivity analysis of g_m to changing Γ^* and electron transport rate (J) of eight *Populus* × *canadensis* Moench genotypes.

Acknowledgements

We thank Stephane Martin and Jean-Charles Olry, members of the Experimental Phytotronic Platform of Lorraine PEPLor, University of Lorraine, for taking care of the ozone facilities and for logistical support throughout the experiment, respectively. This work benefited from the ASIA platform (Université de Lorraine; https://a2f.univ-lorraine.fr/en/asia-2/). Also, many thanks to the ONF nursery in Guéméné-Penfao for providing the cuttings.

Author contributions

RJ and AG performed the experiments and conceived the original idea; AB and RJ carried out the laboratory work; AG and YJ supervised the project; RJ drafted the manuscript; all authors discussed the results and contributed to the final manuscript.

Conflict of interest

The authors declare that the research was conducted in the absence of any commercial or financial relationships that could be construed as a potential conflict of interest.

Funding

RJ was funded by a PhD grant from the Ministère de l'Enseignement Supérieur et de la Recherche. This work was also supported by the French National Research Agency through the Laboratory of Excellence ARBRE (ANR-12-LABXARBRE-01).

Data availability

The data supporting the findings of this study are available from the corresponding author (AG), upon request.

References

Bagard M, Le Thiec D, Delacote E, Hasenfratz-Sauder M-P, Banvoy J, Gérard J, Dizengremel P, Jolivet Y. 2008. Ozone-induced changes in photosynthesis and photorespiration of hybrid poplar in relation to the developmental stage of the leaves. Physiologia Plantarum **134**, 559–574.

Bohler S, Sergeant K, Hoffmann L, Dizengremel P, Hausman J-F, Renaut J, Jolivet Y. 2011. A difference gel electrophoresis study on thylakoids isolated from poplar leaves reveals a negative impact of ozone exposure on membrane proteins. Journal of Proteome Research **10**, 3003–3011.

Bortier K, De Temmerman L, Ceulemans R. 2000. Effects of ozone exposure in open-top chambers on poplar (*Populus nigra*) and beech (*Fagus sylvatica*): A comparison. Environmental Pollution **109**, 509–516.

Bussotti F, Agati G, Desotgiu R, Matteini P, Tani C. 2005. Ozone foliar symptoms in woody plant species assessed with ultrastructural and fluorescence analysis. New Phytologist **166**, 941–955.

Cabané M, Pireaux J-C, LégerE, Weber E, Dizengremel P, Pollet B, Lapierre C. 2004. Condensed lignins are synthesized in poplar leaves exposed to ozone. Plant Physiology **134**, 586–594.

Calatayud V, Marco F, CerveróJ, Sánchez-PeñaG, José SanzM. 2010. Contrasting ozone sensitivity in related evergreen and deciduous shrubs. Environmental Pollution **158**, 3580–3587.

Clemente-Moreno MJ, Gago J, Díaz-Vivancos P, Bernal A, Miedes E, Bresta P, Liakopoulos G, Fernie AR, Antonio Hernández J, Flexas J. 2019. The apoplastic antioxidant system and altered cell wall dynamics influence mesophyll conductance and the rate of photosynthesis. The Plant Journal **99**, 1031–1046.

Dai L, Feng Z, Pan X, Xu Y, Li P, Lefohn AS, Harmens H, Kobayashi K. 2019. Increase of apoplastic ascorbate induced by ozone is insufficient to remove the negative effects in tobacco, soybean and poplar. Environmental Pollution **245**, 380–388.

Di Baccio D, Castagna A, Paoletti E, Sebastiani L, Ranieri A. 2008. Could the differences in O_3 sensitivity between two poplar clones be related to a difference in antioxidant defense and secondary metabolic response to O_3 influx? Tree Physiology **28**, 1761–1772.

Dizengremel P. 2001. Effects of ozone on the carbon metabolism of forest trees. Plant Physiology and Biochemistry **39**, 729–742.

Dizengremel P, Jolivet Y, Tuzet A, Ranieri A, Le Thiec D. 2013. Integrative leaf-level phytotoxic ozone dose assessment for forest risk modelling. In: Matyssek R, Clarke N, Cudlin P, Mikkelsen TN, Tuovinen JP, Wieser G, Paoletti E, eds. Climate change, air pollution and global challenges: Understanding and perspectives from forest research. Developments in Environmental Science, vol. **13**. Elsevier, 267–288.

Dizengremel P, Vaultier M-N, Le Thiec D, *et al*. 2012. Phosphoenolpyruvate is at the crossroads of leaf metabolic responses to ozone stress: Letters. New Phytologist **195**, 512–517.

Dumont J, Cohen D, Gérard J, Jolivet Y, Dizengremel P, Le Thiec D. 2014. Distinct responses to ozone of abaxial and adaxial stomata in three Euramerican poplar genotypes. Plant, Cell & Environment **37**, 2064–2076.

Dusart N, Gandin A, Marie-Noëlle V, Joffe R, Cabané M, Dizengremel P, Jolivet Y. 2019a. Importance of detoxification processes in ozone risk assessment: need to integrate the cellular compartmentation of antioxidants? Frontiers in Forests and Global Change **2**, 45.

Dusart N, Gérard J, Le Thiec D, Collignon C, Jolivet Y, Vaultier MN. 2019b. Integrated analysis of the detoxification responses of two Euramerican poplar genotypes exposed to ozone and water deficit: focus on the ascorbate-glutathione cycle. Science of The Total Environment **651**, 2365–2379.

Duursma RA. 2015. Plantecophys – An R package for analysing and modelling leaf gas exchange data. PLoS One **10**, e0143346.

Elferjani R, Benomar L, Momayyezi M, *et al*. 2021. A meta-analysis of mesophyll conductance to CO_2 in relation to major abiotic stresses in poplar species. Journal of Experimental Botany **72**, 4384–4400.

Emberson LD, Pleijel H, Ainsworth EA, *et al.* 2018. Ozone effects on crops and consideration in crop models. European Journal of Agronomy **100**, 19–34.

Evans JR, Kaldenhoff R, Genty B, Terashima I. 2009. Resistances along the CO_2 diffusion pathway inside leaves. Journal of Experimental Botany **60**, 2235–2248.

Evans JR, von Caemmerer S. 1996. Carbon dioxide diffusion inside leaves. Plant Physiology **110**, 339–346.

Evans JR, Von Caemmerer S. 2013. Temperature response of carbon isotope discrimination and mesophyll conductance in tobacco. Plant, Cell & Environment **36**, 745–756.

Farmer EE, Mueller MJ. 2013. ROS-mediated lipid peroxidation and RES-activated signaling. Annual Review of Plant Biology **64**, 429–450.

Flexas J, Barbour MM, Brendel O, *et al.* 2012. Mesophyll diffusion conductance to CO_2: an unappreciated central player in photosynthesis. Plant Science **193–194**, 70–84.

Flexas J, Clemente-Moreno MJ, Bota J, *et al.* 2021. Cell wall thickness and composition are involved in photosynthetic limitation. Journal of Experimental Botany **11**, 3971–3986.

Flexas J, Javier Cano F, Carriquí M, Coopman RE, Mizokami Y, Tholen D, Xiong D. 2018. CO_2 diffusion inside photosynthetic organs. In: Adams WW III, Terashima I, eds. The leaf: a platform for performing photosynthesis. Advances in photosynthesis and respiration, vol. **44**. Cham: Springer International Publishing, 163–208.

Flexas J, Ribas-CarbóM, Diaz-Espejo A, GalmésJ, Medrano H. 2008. Mesophyll conductance to CO_2: current knowledge and future prospects. Plant, Cell & Environment **31**, 602–621.

Force L, Critchley C, van Rensen JJ. 2003. New fluorescence parameters for monitoring photosynthesis in plants. Photosynthesis Research **78**, 17.

Fowler D, Amann M, Anderson R, *et al.* 2008. Ground-level ozone in the 21st century: future trends, impacts and policy implications. London: The Royal Society. http://royalsociety.org/policy/publications/2008/ground-level-ozone/

Gago J, Daloso DM, Carriquí M, Nadal M, Morales M, Araújo WL, Nunes-Nesi A, Flexas J. 2020. Mesophyll conductance: the leaf corridors for photosynthesis. Biochemical Society Transactions **48**, 429–439.

Genty B, Briantais J-M, Baker NR. 1989. The relationship between the quantum yield of photosynthetic electron transport and quenching of chlorophyll fluorescence. Biochimica et Biophysica Acta – General Subjects **990**, 87–92.

Gerosa G, Marzuoli R, Bussotti F, Pancrazi M, Ballarin-Denti A. 2003. Ozone sensitivity of *Fagus sylvatica* and *Fraxinus excelsior* young trees in relation to leaf structure and foliar ozone uptake. Environmental Pollution, **125**, 91–98.

Gill SS, Tuteja N. 2010. Reactive oxygen species and antioxidant machinery in abiotic stress tolerance in crop plants. Plant Physiology and Biochemistry **48**, 909–930.

Grassi G, Magnani F. 2005. Stomatal, mesophyll conductance and biochemical limitations to photosynthesis as affected by drought and leaf ontogeny in ash and oak trees. Plant, Cell & Environment **28**, 834–849.

Gu L, Sun Y. 2014. Artefactual responses of mesophyll conductance to CO_2 and irradiance estimated with the variable J and online isotope discrimination methods. Plant, Cell & Environment **37**, 1231–1249.

Günthardt-Goerg MS. 1996. Different responses to ozone of tobacco, poplar, birch, and alder. Journal of Plant Physiology **148**, 207–214.

Haberer K, Herbinger K, Alexou M, Tausz M, Rennenberg H. 2007. Antioxidative defence of old growth beech (*Fagus sylvatica*) under double ambient O_3 concentrations in a free-air exposure system. Plant Biology **9**, 215–226.

Harley PC, Loreto F, Di Marco G, Sharkey TD. 1992. Theoretical considerations when estimating the mesophyll conductance to CO_2 flux by analysis of the response of photosynthesis to CO_2. Plant Physiology **98**, 1429–1436.

Harmens H, Hayes F, Sharps K, Mills G, Calatayud V. 2017. Leaf traits and photosynthetic responses of *Betula pendula* saplings to a range of ground-level ozone concentrations at a range of nitrogen loads. Journal of Plant Physiology **211**, 42–52.

Heath RL. 2008. Modification of the biochemical pathways of plants induced by ozone: what are the varied routes to change? Environmental Pollution, **155**, 453–463.

Herschbach C, Teuber M, Eiblmeier M, ehlting B, Ache P, Polle A, Schnitzler J-P, Rennenberg H. 2010. Changes in sulphur metabolism of grey poplar (*Populus* × *canescens*) leaves during salt stress: a metabolic link to photorespiration. Tree Physiology **30**, 1161–1173.

Hörtensteiner S. 1999. Chlorophyll breakdown in higher plants and algae. Cellular and Molecular Life Sciences **56**, 330–347.

Hoshika Y, Haworth M, Watanabe M, Koike T. 2020. Interactive effect of leaf age and ozone on mesophyll conductance in Siebold's beech. Physiologia Plantarum, 13121.

Hothorn T, Bretz F, Hothorn MT. 2009. The multcomp package. R Project for Statistical Computing.

Jolivet Y, Bagard M, CabanéM, Vaultier M-N, Gandin A, Afif D, Dizengremel P, Le Thiec D. 2016. Deciphering the ozone-induced changes in cellular processes: a prerequisite for ozone risk assessment at the tree and forest levels. Annals of Forest Science **73**, 923–943.

Kassambara A. 2020. rstatix: Pipe-friendly framework for basic statistical tests. R package version 0.6.0.

Kassambara A, Kassambara MA. 2020. Package 'ggpubr'. R package version 0.1, 6.

Knauer J, Zaehle S, De Kauwe MG, Bahar NHA, Evans JR, Medlyn BE, Reichstein M, Werner C. 2019. Effects of mesophyll conductance on vegetation responses to elevated CO_2 concentrations in a land surface model. Global Change Biology **25**, 1820–1838.

Knauer J, Zaehle S, De Kauwe MG, Haverd V, Reichstein M, Sun Y. 2020. Mesophyll conductance in land surface models: effects on photosynthesis and transpiration. The Plant Journal **101**, 858–873.

Kronfuß G, Polle A, Tausz M, Havranek WM, Wieser G. 1998. Effects of ozone and mild drought stress on gas exchange, antioxidants and chloroplast pigments in current-year needles of young Norway spruce [*Picea abies* (L.) Karst.]. Trees **12**, 482–489.

Laisk A, Loreto F. 1996. Determining photosynthetic parameters from leaf CO_2 exchange and chlorophyll fluorescence (ribulose-1,5-bisphosphate carboxylase/oxygenase specificity factor, dark respiration in the light, excitation distribution between photosystems, alternative electron transport rate, and mesophyll diffusion resistance. Plant Physiology **110**, 903–912.

Lawson T, Vialet-Chabrand S. 2019. Speedy stomata, photosynthesis and plant water use efficiency. New Phytologist **221**, 93–98.

Lenth R, Singmann H, Love J, Buerkner P, Herve M .2018. Emmeans: Estimated marginal means, aka least-squares means. R package version, **1**(1), 3.

Li P, Calatayud V, Gao F, Uddling J, Feng Z. 2016. Differences in ozone sensitivity among woody species are related to leaf morphology and antioxidant levels. Tree Physiology **36**, 1105–1116.

Loreto F, Mannozzi M, Maris C, Nascetti P, Ferranti F, Pasqualini S. 2001. Ozone quenching properties of isoprene and its antioxidant role in leaves. Plant Physiology **126**, 993–1000.

Loriaux SD, Avenson TJ, Welles JM, Mcdermitt DK, Eckles RD, Riensche B, Genty B. 2013. Closing in on maximum yield of chlorophyll fluorescence using a single multiphase flash of sub-saturating intensity. Plant, Cell & Environment **36**, 1755–1770.

Mattila H, Valev D, Havurinne V, Khorobrykh S, Virtanen O, Antinluoma M, Mishra K, Tyystjärvi E. 2018. Degradation of chlorophyll and synthesis of flavonols during autumn senescence—the story told by individual leaves. AoB Plants **10**, ply028.

Milla-Moreno EA, McKown AD, Guy RD, Soolanayakanahally RY. 2016. Leaf mass per area predicts palisade structural properties linked to mesophyll conductance in balsam poplar (*Populus Balsamifera* L.). Botany **94**, 225–239.

Moldau H. 1998. Hierarchy of ozone scavenging reactions in the plant cell wall. Physiologia Plantarum **104**, 617–622.

Monclus R, Dreyer E, Villar M, Delmotte FM, Delay D, Petit J-M, Barbaroux C, Le Thiec D, BréchetC, Brignolas F. 2006. Impact of drought on productivity and water use efficiency in 29 genotypes of *Populus deltoides* × *Populus nigra*. New Phytologist **169**, 765–777.

Morales M, Munné-BoschS. 2019. Malondialdehyde: facts and artifacts. Plant Physiology **180**, 1246–1250.

Murchie EH, Lawson T. 2013. Chlorophyll fluorescence analysis: a guide to good practice and understanding some new applications. Journal of Experimental Botany **64**, 3983–3998.

Noctor G, Reichheld JP, Foyer CH. 2018. ROS-related redox regulation and signaling in plants. Seminars in Cell & Developmental Biology **80**, 3–12.

Noormets A, Sober A, Pel EJ, Dickson RE, Podila GK, Sober J, Isebrands JG, Karnosky DF. 2001. Stomatal and non-stomatal limitation to photosynthesis in two trembling aspen (*Populus tremuloides* Michx.) clones exposed to elevated CO_2 and/or O_3. Plant, Cell & Environment, **24**, 327–336.

Oksanen E, Riikonen J, Kaakinen S, Holopainen T, Vapaavuori E. 2005. Structural characteristics and chemical composition of birch (*Betula pendula*) leaves are modified by increasing CO_2 and ozone. Global Change Biology **11**, 732–748.

Oksanen E, Sober J, Karnosky DF. 2001. Impacts of elevated CO_2 and/or O_3 on leaf ultrastructure of aspen (*Populus tremuloides*) and birch (*Betula papyrifera*) in the aspen FACE experiment. Environmental Pollution **115**, 437–446.

Onoda Y, Wright IJ, Evans JR, Hikosaka K, Kitajima K, Niinemets U, Poorter H, Tosens T, Westoby M. 2017. Physiological and structural tradeoffs underlying the leaf economics spectrum. New Phytologist **214**, 1447–1463.

Paoletti E, Contran N, Bernasconi P, Günthardt-Goerg MS, Vollenweider P. 2009. Structural and physiological responses to ozone in manna ash (*Fraxinus ornus* L.) leaves of seedlings and mature trees under controlled and ambient conditions. Science of The Total Environment **407**, 1631–1643.

Paoletti E, Feng Z, De Marco A, *et al.* 2020. Challenges, gaps and opportunities in investigating the interactions of ozone pollution and plant ecosystems. Science of The Total Environment **709**, 136188.

Paoletti E, Grulke NE (2010). Ozone exposure and stomatal sluggishness in different plant physiognomic classes. Environmental Pollution **158**, 2664–2671.

Pell EJ, Eckardt N, Enyedi AJ. 1992. Timing of ozone stress and resulting status of ribulose bisphosphate carboxylase/oxygenase and associated net photosynthesis. New Phytologist **120**, 397–405.

Pell, EJ, Schlagnhaufer CD, Arteca RN. 1997. Ozone-induced oxidative stress: mechanisms of action and reaction. Physiologia Plantarum **100**, 264–273.

Pons TL, Flexas J, von Caemmerer S, Evans JR, Genty B, Ribas-Carbo M, Brugnoli E. 2009. Estimating mesophyll conductance to CO_2: methodology, potential errors, and recommendations. Journal of Experimental Botany **60**, 2217–2234.

Proietti C, Anav A, De Marco A, Sicard P, Vitale M. 2016. A multi-sites analysis on the ozone effects on gross primary production of European forests. Science of The Total Environment **556**, 1–11.

Ranieri A, Giuntini D, Ferraro F, Nali C, Baldan B, Lorenzini G, Franco Soldatini G. 2001. Chronic ozone fumigation induces alterations in thylakoid functionality and composition in two poplar clones. Plant Physiology and Biochemistry **39**, 999–1008.

R Core Team. 2018. R: A language and environment for statistical computing. Vienna, Austria: R Foundation for Statistical Computing.

Reid CD, Fiscus EL, Burkey KO. 1998. Combined effects of chronic ozone and elevated CO_2 on Rubisco activity and leaf components in soybean (*Glycine max*). Journal of Experimental Botany **49**, 1999–2011.

Saitanis CJ, Riga-Karandinos AN, Karandinos MG. 2001. Effects of ozone on chlorophyll and quantum yield of tobacco (*Nicotiana tabacum* L.) varieties. Chemosphere **42**, 945–953.

Schaub M, Haeni M, Calatayud V. 2018. Ozone concentrations are decreasing but exposure remains high in European forests. ICP Forests Brief, vol. 3. Eberswalde: Thünen Institute of Forest Ecosystems. https://doi.org/10.3220/ICP1525258743000.

Shang B, Feng ZZ, Gao F, Calatayud V. 2020. The ozone sensitivity of five poplar clones is not related to stomatal conductance, constitutive antioxidant levels and morphology of leaves. Science of The Total Environment **699**, 134402.

Sicard P, Anav A, De Marco A, Paoletti E. 2017. Projected global ground-level ozone impacts on vegetation under different emission and climate scenarios. Atmospheric Chemistry and Physics **17**, 12177–12196.

Soolanayakanahally RY, Guy RD, Silim SN, Drewes EC, Schroeder WR. 2009. Enhanced assimilation rate and water use efficiency with latitude through increased photosynthetic capacity and internal conductance in balsam poplar (*Populus balsamifera* L.). Plant, Cell & Environment **32**, 1821–1832.

South PF, Cavanagh AP, Liu HW, Ort DR. 2019. Synthetic glycolate metabolism pathways stimulate crop growth and productivity in the field. Science **363**, eaat9077.

Sugiura D, Terashima I, Evans JR. 2020. A decrease in mesophyll conductance by cell-wall thickening contributes to photosynthetic downregulation. Plant Physiology **183**, 1600–1611.

Sun Y, Gu L, Dickinson RE, Norby RJ, Pallardy SG, Hoffman FM. 2014a. Impact of mesophyll diffusion on estimated global land CO_2 fertilization. Proceedings of the National Academy of Sciences, USA **111**, 15774–15779.

Sun Y, Gu L, Dickinson RE, *et al*. 2014b. Asymmetrical effects of mesophyll conductance on fundamental photosynthetic parameters and their relationships estimated from leaf gas exchange measurements. Plant, Cell & Environment **37**, 978–994.

Tagnon MD, Simeon KO. 2017. Aldehyde dehydrogenases may modulate signaling by lipid peroxidation-derived bioactive aldehydes. Plant Signaling & Behavior **12**, e1387707.

Terashima I, Hanba YT, Tholen D, Niinemets U. 2011. Leaf functional anatomy in relation to photosynthesis. Plant Physiology **155**, 108–116.

Théroux Rancourt G, Éthier G, Pepin S. 2015. Greater efficiency of water use in poplar clones having a delayed response of mesophyll conductance to drought. Tree Physiology **35**, 172–184.

Tholen D, Boom C, Noguchi K, Ueda S, Katase T, Terashima I. 2008. The chloroplast avoidance response decreases internal conductance to CO_2 diffusion in *Arabidopsis thaliana* leaves. Plant, Cell & Environment **31**, 1688–1700.

Tosens T, Niinemets UL, Vislap V, Eichelmann H, Castro Díez P. 2012. Developmental changes in mesophyll diffusion conductance and photosynthetic capacity under different light and water availabilities in *Populus tremula*: how structure constrains function: structural limitations to photosynthesis. Plant, Cell & Environment **35**, 839–856.

Veromann-Jürgenson L-L, Tosens T, Laanisto L, Niinemets U. 2017. Extremely thick cell walls and low mesophyll conductance: welcome to the world of ancient living! Journal of Experimental Botany **68**, 1639–1653.

von Caemmerer S, Evans JR, Hudson GS, John Andrews T. 1994. The kinetics of ribulose-1,5-bisphosphate carboxylase/oxygenase in vivo inferred from measurements of photosynthesis in leaves of transgenic tobacco. Planta **195**, 88–97.

Walker B, Ariza LS, Kaines S, Badger MR, Cousins AB. 2013. Temperature response of in vivo Rubisco kinetics and mesophyll conductance in *Arabidopsis thaliana*: comparisons to *Nicotiana tabacum*. Plant, Cell & Environment **36**, 2108–2119.

Warren C. 2006. Estimating the internal conductance to CO_2 movement. Functional Plant Biology **33**, 431–442.

Warren CR, Dreyer E. 2006. Temperature response of photosynthesis and internal conductance to CO_2: results from two independent approaches. Journal of Experimental Botany **57**, 3057–3067.

Wittig VE, Ainsworth EA, Long SP. 2007. To what extent do current and projected increases in surface ozone affect photosynthesis and stomatal conductance of trees? A meta-analytic review of the last 3 decades of experiments. Plant, Cell & Environment **30**, 1150–1162.

Wittig VE, Ainsworth EA, Naidu SL, Karnosky DF, Long SP. 2009. Quantifying the impact of current and future tropospheric ozone on tree

biomass, growth, physiology and biochemistry: a quantitative meta-analysis. Global Change Biology **15**, 396–424.

Wright IJ, Reich PB, Cornelissen JHC, *et al*. 2005. Modulation of leaf economic traits and trait relationships by climate. Global Ecology and Biogeography **14**, 411–421.

Xu Y, Feng ZZ, Shang B, Dai L, Uddling J, Tarvainen L. 2019. Mesophyll conductance limitation of photosynthesis in poplar under elevated ozone. Science of The Total Environment **657**, 136–145.

Xu Y, Shang B, Feng Z, Tarvainen L. 2020. Effect of elevated ozone, nitrogen availability and mesophyll conductance on the temperature responses of leaf photosynthetic parameters in poplar. Tree Physiology **40**, 484–497.

Ye M, Zhang Z, Huang G, Xiong Z, Peng S, Li Y. 2020. High leaf mass per area *Oryza* genotypes invest more leaf mass to cell wall and show a low mesophyll conductance. AoB Plants **12**, plaa028.

Zechmann B. 2011. Subcellular distribution of ascorbate in plants. Plant Signaling & Behavior **6**, 360–363.

Zhang JJ, Wei Y, Fang Z. 2019. Ozone pollution: a major health hazard worldwide. Frontiers in Immunology **10**, 2518.

Zhu X, Jiang J, Yin C, Li G, Jiang Y, Shan Y. 2019. Effect of ozone treatment on flavonoid accumulation of satsuma mandarin (*Citrus unshiu* Marc.) during ambient storage. Biomolecules **9**, 821.